**Supplementary Information**

**for**

# Mechanistic Origin of Charge Separation and Enhanced Photocatalytic Activity in D–π–A-Functionalized UiO-66-$NH_2$ MOFs

Anastasiia Kultaeva[1], Volodymyr Vasylkovskyi[1], Andreas Sperlich[1], Eugenio Otal[2], Katsuya Teshima[2,3,4], Wolf Gero Schmidt[5], Timur Biktagirov[5]

[1]*Experimental Physics 6 and Würzburg-Dresden Cluster of Excellence ct.qmat, Julius-Maximilian University of Würzburg, 97074 Würzburg, German*

[2]*Institute for Aqua Regeneration (ARG), Shinshu University, 4-17-1 Wakasato, Nagano 380-8553, Japan*

[3]*Department of Materials Chemistry, Faculty of Engineering, Shinshu University, 4-17-1 Wakasato, Nagano 380-8553, Japan*

[4]*Research Initiative for Supra-Materials (RISM), Interdisciplinary Cluster for Cutting Edge Research (ICCER), Shinshu University, Nagano 380-8553, Japan*

[5]*Physics Department, Paderborn University, D-33098 Paderborn, Germany*

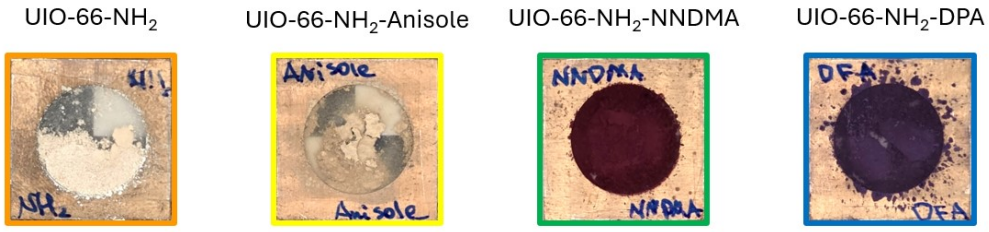


**Figure S1.** Optical photographs of pristine UIO-66-$NH_2$ and linker-modified (-Anisole, -NNDMA, and -DPA) powder samples mounted in sample holders for PL and trPL measurements.

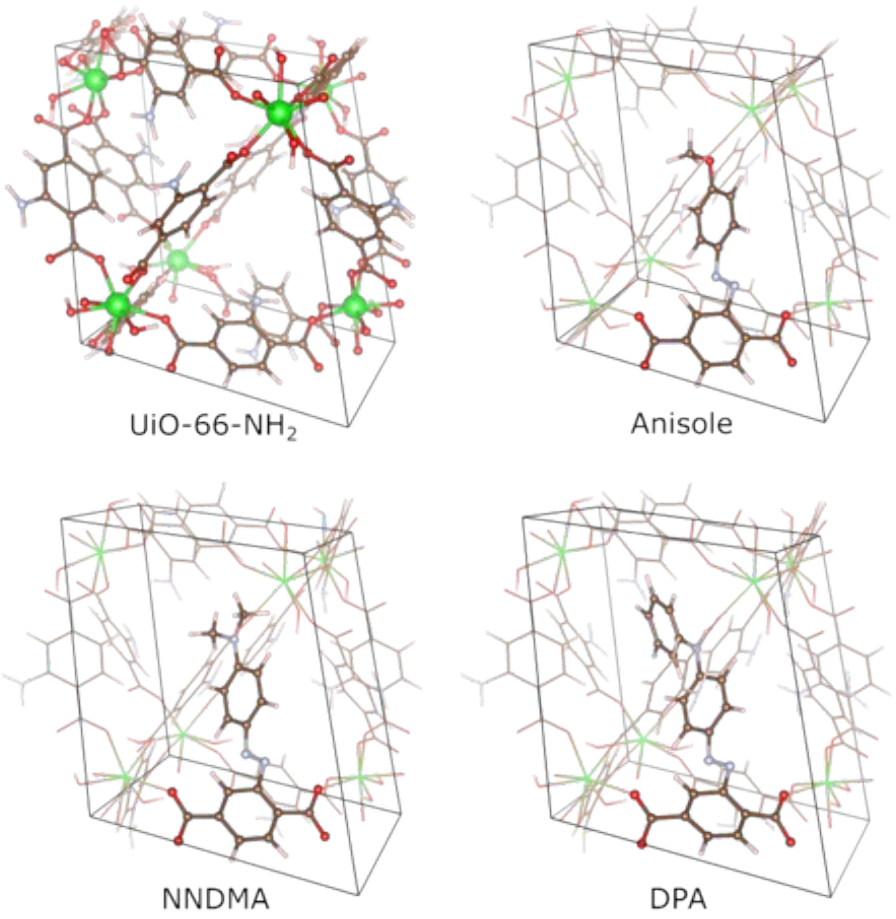


**Figure S2.** DFT-optimized supercell models of non-modified and diazo-coupled UiO-66–$NH_2$ (color key: carbon, brown; oxygen, red; hydrogen, white; nitrogen, grey; and zirconium, green).

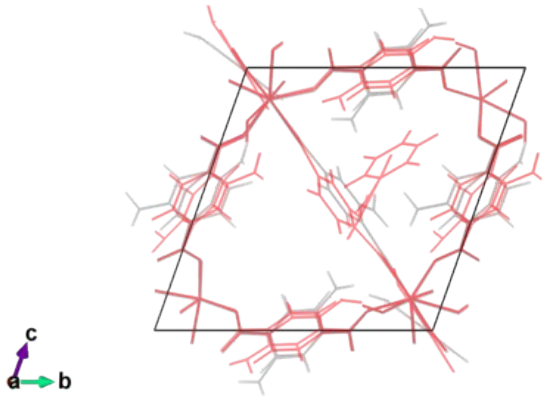


**Figure S3.** Overlay of the nonmodified (grey) and DPA-coupled (red) UiO-66-$NH_2$ DFT-optimized structures illustrating the distortions caused by the introduction of the functional group.

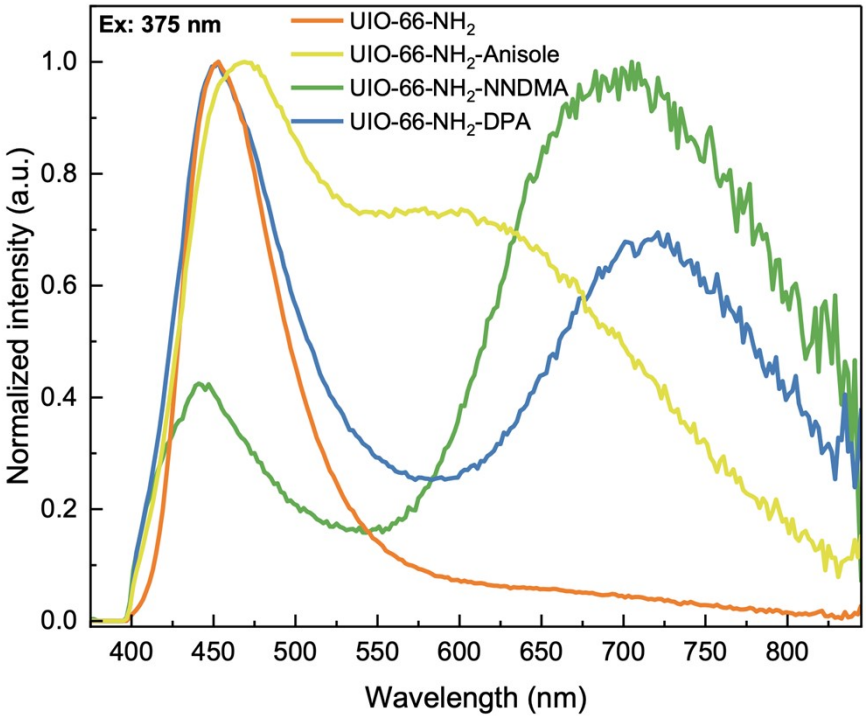


**Figure S4.** Normalized PL spectra of pristine and modified UIO-66-$NH_2$ in the 375 – 845 nm range. The dual emission character of the loaded structures is indicative of incomplete loading by diazo-functionalization. Significant part of the UiO-66-$NH_2$ remains non modified.

The UIO-66-$NH_2$-Anisole sample exhibits a ~16 nm red shift of the main UIO-66-$NH_2$ peak from 467 nm, accompanied by peak broadening. An additional broad emission band appears near 600 nm, with an intensity approximately 20% lower than that of the main peak. UIO-66-$NH_2$-NNDMA displays a ~10 nm blue shift of the UIO-66-$NH_2$ characteristic emission peak to 442 nm, along with the appearance of a broad, intense emission at 700 nm, roughly twice the intensity of the 441 nm peak. The UIO-66-$NH_2$-DPA shows retention of the main emission peak at 451 nm, but with slight peak broadening and an additional broad feature near 715 nm, ~25% lower in intensity than the 451 nm emission. PL results demonstrate that D–π–A linker incorporation strongly affects the optical transitions in UiO-66-$NH_2$, leading to new emission channels and spectral shifts. A detailed graph of peak shifts is shown in Figure S8.

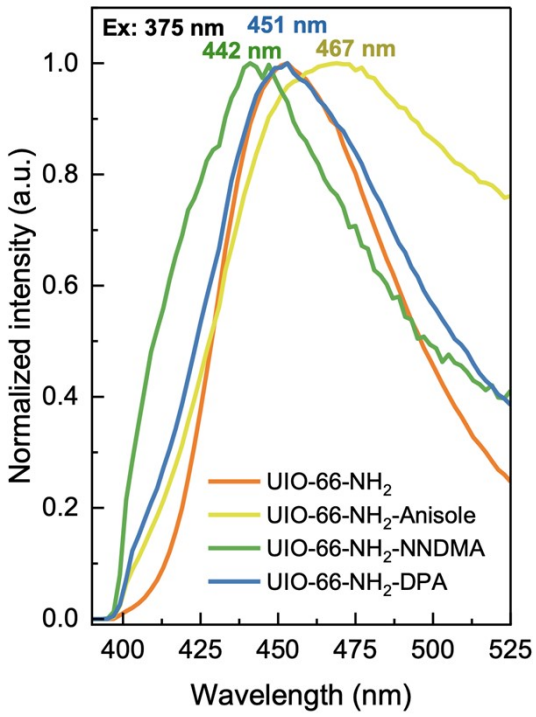


**Figure S5.** Normalized PL spectra of pristine and modified UIO-66-$NH_2$ in the 380–525 nm range.

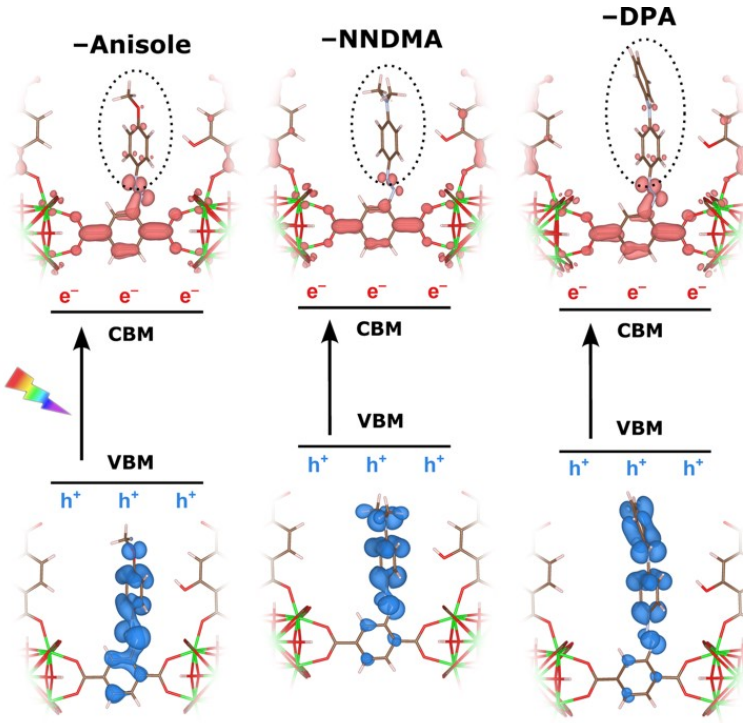


**Figure S6**. Visualization of the highest occupied and lowest unoccupied states in dye-modified systems, showing spatial separation of the photoexcited electron (mainly on the linker backbone) and the hole (localized on the dye and azo bridge).

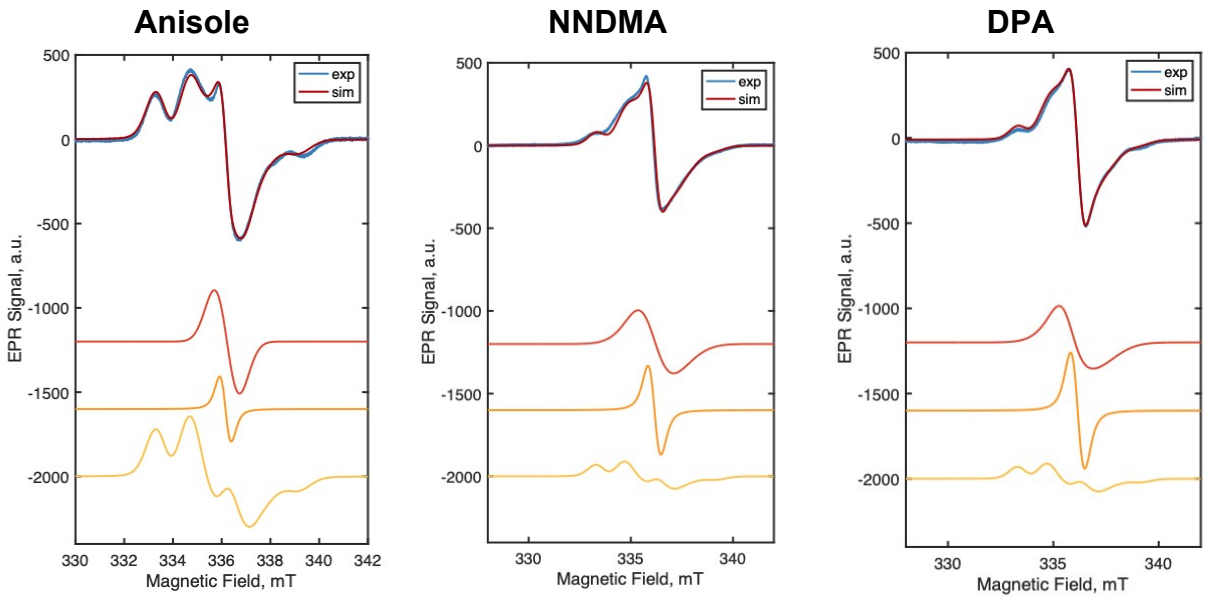


**Figure S7.** EPR simulations for dye-modified MOFs. The EasySpin parameters of the three superimposed spectral components are listed in Table S1.

**Table S1**. EasySpin parameters of the spectral components used in the EPR simulations in Figure S7

| | Parameter | Anisole | NNDMA | DPA |
|---|---|---|---|---|
| Species 1 | g<br>lw<br>weight | 2.0042<br>[0.4, 0.4]<br>0.037 | 2.0042<br>[0.5, 0.6]<br>0.40 | 2.0042<br>[0.55, 0.6]<br>0.55 |
| Species 2 | g<br>gStrain<br>lw<br>weight | [2.0025, 2.0025, 2.0066]<br>[0.003, 0.003, 0.002]<br>1.0<br>0.15 | [2.0025, 2.0025, 2.0051]<br>[0.015, 0.015, 0.006]<br>1.0<br>1.30 | [2.0025, 2.0025, 2.0066]<br>[0.015, 0.015, 0.001]<br>1.0<br>1.20 |
| NH• | weight | 1.00<br>for the EasySpin parameters of the NH• radical, see Ref. [20] of the main text | | |

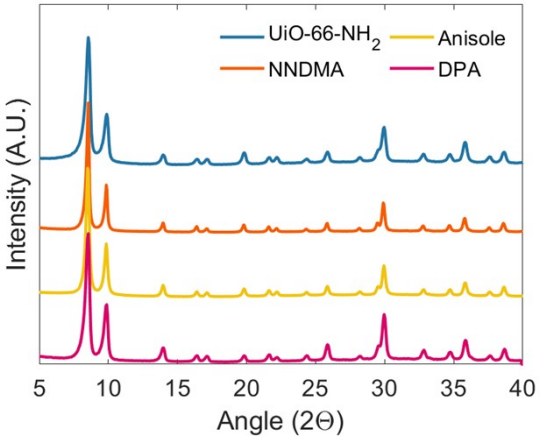


**Figure S8.** Powder X-ray diffractograms of dye-modified frameworks compared to the pristine UiO-66–$NH_2$ reference. These results confirm that the samples retain crystallinity after diazo coupling.

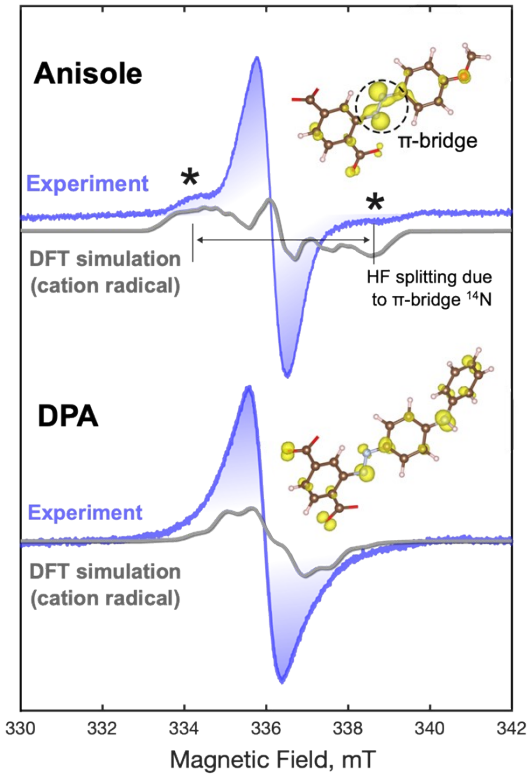


**Figure S9.** Comparison between experimental photoinduced EPR spectra for anisole- and DPA-functionalized samples (cf. Figure 3C in the main text) and simulated spectra for a model cation radical localized on functionalized linkers. Grey curves correspond to spectra simulated using EPR parameters (*g*-tensors and hyperfine coupling tensors with all $^{14}N$ and $^{1}H$ nuclei of the functionalized linkers) obtained directly from DFT calculations for the models shown in the insets (anisole- and DPA-modified BDC linkers with a +1 charge added to simulate a photoinduced hole stabilized after charge separation). For anisole, the calculated spin density (shown in the insets as a yellow isosurface) is substantially localized on the –N=N– π-bridge, resulting in sizeable hyperfine coupling. The largest hyperfine tensor principal values are [14.56, 16.65, 51.97] MHz for one of the bridge nitrogens (nuclear spin $I = 1$), leading to the splitting consistent with the satellite features observed experimentally (marked by asterisks). For DPA, the spin density is more delocalized, and the largest hyperfine coupling is substantially smaller ([25.60, −3.65, −3.64] MHz) so that the simulated spectrum remains within the broad experimental EPR line. Note that in both cases these signals are likely superimposed with contributions from other photogenerated spin centers responsible for the central line [7].

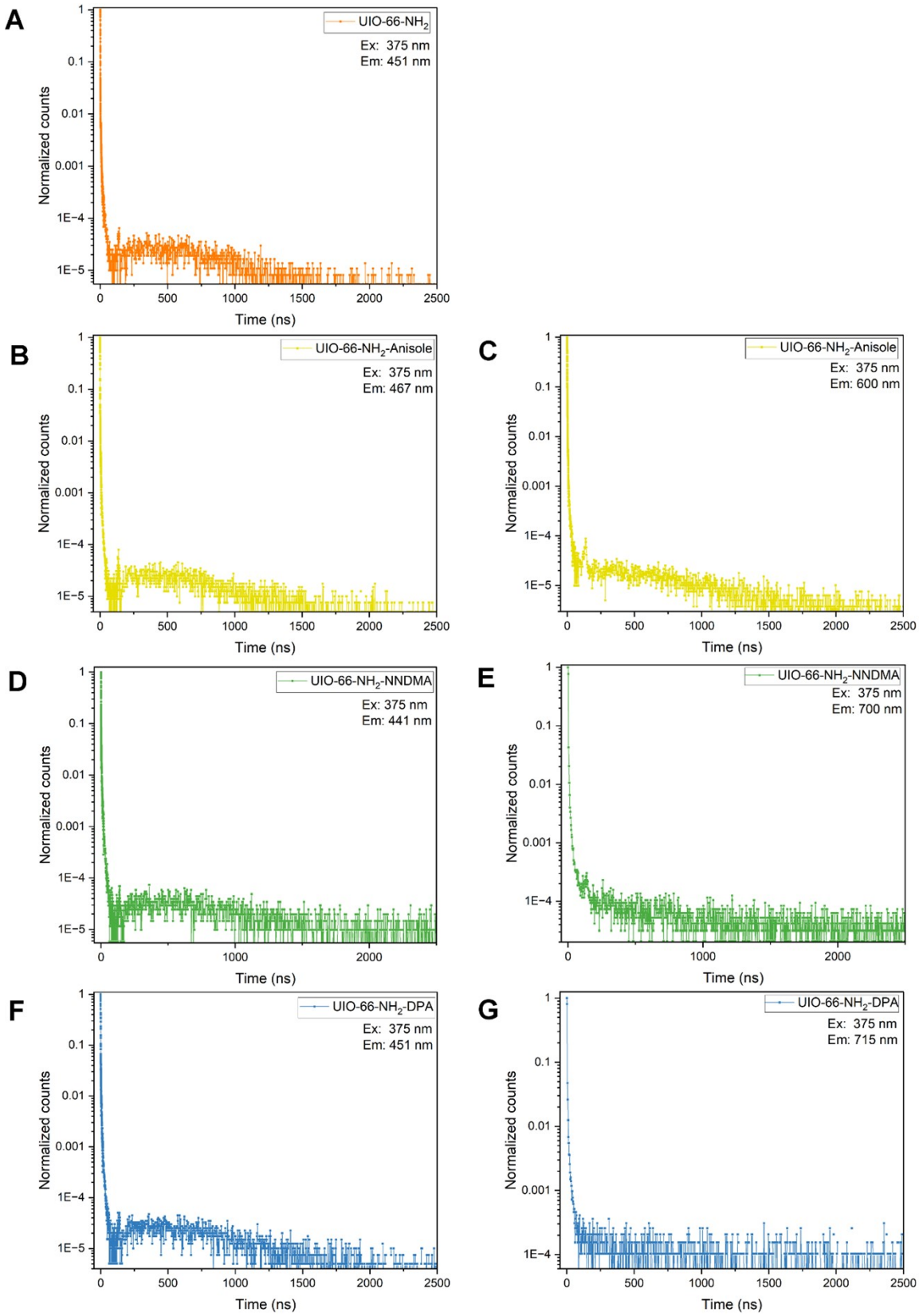


**Figure S10.** Time-resolved PL decay of (A) UIO-66-$NH_2$ at 451 nm; UIO-66-$NH_2$-Anisole at (B) 467 nm and (C) 600 nm; UIO-66-$NH_2$-NNDMA at (D) 441 nm and (E) 700 nm; UIO-66-$NH_2$-DPA at (F) 451 nm and (G) 715 nm emission wavelength. Since the dye-modified samples exhibit two PL peaks (cf. Figure S5) – 1$^{st}$ originating from the fraction of UiO-66-$NH_2$ parent framework and 2$^{nd}$ related to fraction with the respective linker modification – both regions were probed separately to analyze their individual recombination behaviors.

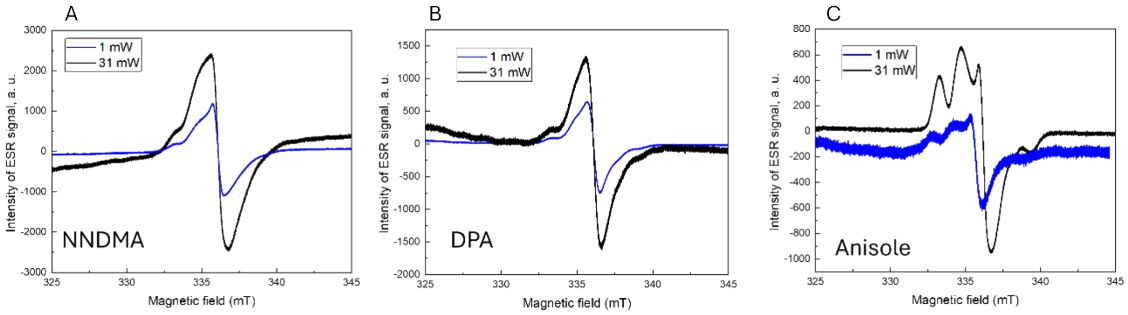


**Figure S11.** The microwave power dependence of EPR signals for dye-functionalized MOFs at the 293 K. The almost identical behaviour under two different microwave power settings displays the same spin-spin and spin-lattice relaxation times for the different species contributing to the superimposed spectra.

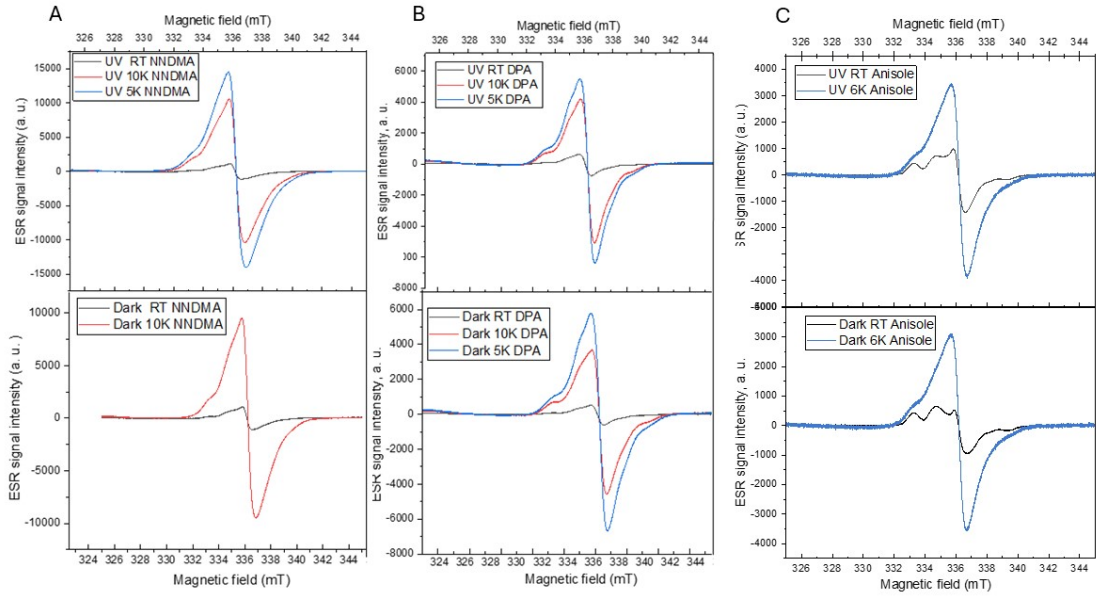


**Figure S12.** The temperature dependence of EPR signals for dye-functionalized MOFs at 1 mW microwave power. The temperature dependence demonstrates a homogeneous increase in the intensities of the spectra for NNDMA and DPA modifications indicating relatively long relaxation times of the paramagnetic centers which are not significantly temperature-dependent. In the case of the Anisole-modified spectra at room temperature, the spectrum from ·NH groups dominates, but the low-temperature spectrum is identical to the modifications described above. This confirms the formation of radicals of the same nature in all the modified samples.